
This is an electronic reprint of the original article.
This reprint may differ from the original in pagination and typographic detail.

Karttunen, Antti J.; Tynell, Tommi; Karppinen, Maarit

Atomic-level structural and electronic properties of hybrid inorganic-organic ZnO:hydroquinone superlattices fabricated by ALD/MLD

Published in:
Journal of Physical Chemistry C

DOI:
[10.1021/acs.jpcc.5b03433](https://doi.org/10.1021/acs.jpcc.5b03433)

Published: 01/01/2015

Document Version
Peer-reviewed accepted author manuscript, also known as Final accepted manuscript or Post-print

Published under the following license:
Unspecified

Please cite the original version:
Karttunen, A. J., Tynell, T., & Karppinen, M. (2015). Atomic-level structural and electronic properties of hybrid inorganic-organic ZnO:hydroquinone superlattices fabricated by ALD/MLD. *Journal of Physical Chemistry C*, 119(23), 13105-13114. <https://doi.org/10.1021/acs.jpcc.5b03433>

This material is protected by copyright and other intellectual property rights, and duplication or sale of all or part of any of the repository collections is not permitted, except that material may be duplicated by you for your research use or educational purposes in electronic or print form. You must obtain permission for any other use. Electronic or print copies may not be offered, whether for sale or otherwise to anyone who is not an authorised user.

Atomic-Level Structural and Electronic Properties of Hybrid Inorganic-Organic ZnO:Hydroquinone Superlattices Fabricated by ALD/MLD

Antti J. Karttunen^{*}, *Tommi Tynell*, and *Maarit Karppinen*

Department of Chemistry, Aalto University, FI-00076 Aalto, Finland

Keywords: Inorganic-organic interfaces, Layered materials, Zinc oxide, Band structure engineering, Ab initio calculations

We investigate crystalline ZnO:hydroquinone (HQ) superlattices grown layer-by-layer by the combined atomic/molecular layer deposition (ALD/MLD) technique; such ALD/MLD layer-engineered inorganic-organic thin films form a fundamentally new category of functional coherent hybrid materials that cannot be prepared by any other existing technique. Using quantum chemical methods, we derive atomic-level structural models for the ZnO:HQ superlattices and investigate their structural, spectroscopic, and electronic properties. By comparing the theoretical results with our experimental data we provide a detailed interpretation of experimentally measured infrared spectra, proving the presence of organic interfaces within the crystalline ZnO:HQ superlattices. We moreover show how the band structure of the hybrid material can be tailored by simple and experimentally feasible modifications of the organic constituent. The guidelines for the band-structure engineering of ZnO:HQ superlattices should be valuable for the systematic enhancement and exploitation of the functional properties of ALD/MLD-grown inorganic-organic superlattices and nanolaminates in general.

^{*} To whom correspondence should be addressed. E-mail: antti.j.karttunen@iki.fi

Introduction

New ground-breaking materials are key enablers of the next-generation advanced technologies. The quest in new-material search is particularly for materials with novel and often unorthodox combinations of properties. Inorganic-organic hybrids combine the best parts of the two worlds, inorganics and organics, and have capacity to open up totally new horizons *e.g.* in flexible electronics, optics, ionics, mechanics, and in various energy, biological and medical applications. The first commercial applications are from 1950s. In the most demanded hybrid materials the inorganic and organic entities would be combined on an atomic/molecular scale, but synthesis of such materials is not straightforward; in fact, a majority of the attractive material characteristics anticipated for these hybrids may not necessarily be achieved for materials fabricated by the contemporary methods.

An elegant way to link inorganic and organic entities *via* strong chemical bonds to form coherent single-phase hybrid materials is to mimic the state-of-the-art gas-phase thin-film deposition technique, *i.e.* ALD (Atomic Layer Deposition), for inorganic materials.¹⁻³ For the inorganic-organic hybrids, ALD cycles are combined with MLD (Molecular Layer Deposition) cycles based on purely organic precursors,⁴⁻⁷ as schematically shown in Figure 1. This enables the atomic/molecular layer-by-layer production of inorganic-organic hybrid thin films through sequential self-limiting gas-surface reactions with high precision for the film thickness and composition like in the case of inorganic ALD thin films. The resultant inorganic-organic hybrid thin films form a fundamentally new category of functional materials that cannot be prepared by any other existing technique. Due to the ample interest in ALD/MLD, the range of materials fabricated by the technique is rapidly increasing.⁸

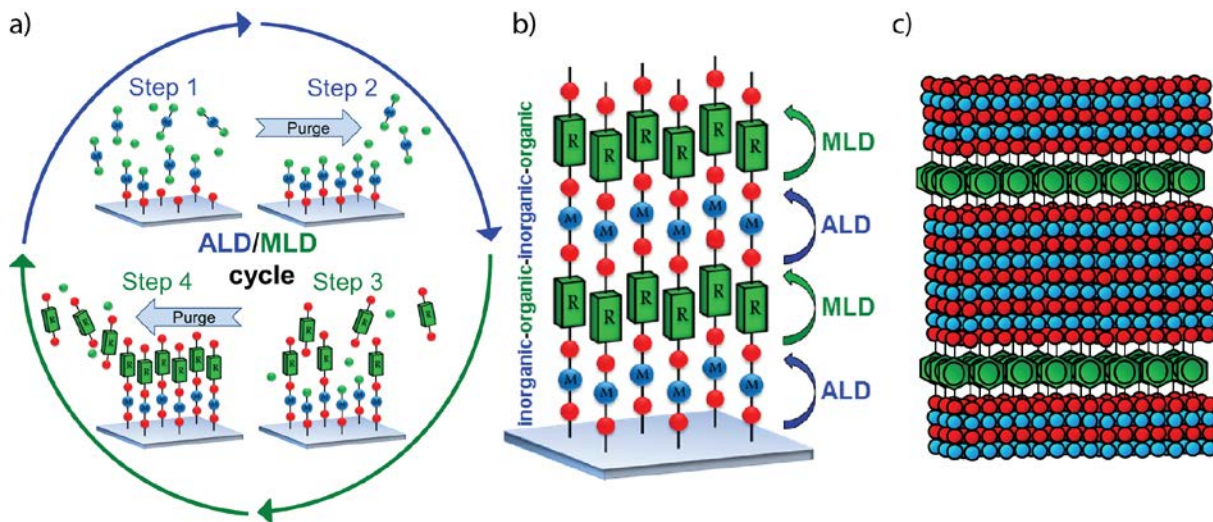


Figure 1. a) An ALD/MLD cycle consisting of four individual steps: (1) pulsing of the inorganic metal (M) precursor, (2) purging with inert gas, (3) pulsing of the organic (R) precursor, and (4) purging with inert gas. b) A schematic structure of a 1:1 hybrid inorganic-organic thin film fabricated by the ALD/MLD technique. c) A schematic structure of an inorganic-organic superlattice thin film deposited by controlling the sequence of the individual ALD and MLD cycles (blue = metal, red = oxygen, green = organic).

Once an ALD/MLD process works ideally⁹ it is relatively straightforward to control the individual inorganic and organic layer thicknesses in a digital manner and thus design and fabricate elaborate layer-engineered materials such as inorganic-organic superlattice thin films (Figure 1c). At the same time it should be emphasized that this is far from straightforward if not impossible with the conventional synthesis methods of hybrid thin films. Superlattices are anticipated to show unusual properties when the thicknesses of individual layers fall below the length scale that characterizes the physical property concerned; for example thermal conductivity is expected to be reduced when the individual layer thickness is less than the mean free path of phonons. This has been shown for purely inorganic nanolaminates¹⁰ and very recently also for ALD/MLD hybrid superlattices prepared at our laboratory.¹¹ Likewise, the motion of charge carriers in nanostructures is often different (*i.e.* the mobility is enhanced) from the motion in the same material in bulk form. Also shown for purely inorganic superstructures is that due to carrier confinement in thin conducting layers Seebeck coefficient may be anomalously increased.¹² Preliminary studies have

also demonstrated interesting optical phenomena for ALD/MLD hybrid thin films, such as sensitization of nanoscale TiO₂ layers to absorption of visible light.¹³ This could be beneficial in applications such as photocatalysis and solar cells, particularly since the ALD/MLD technique (like conventional ALD) would inherently allow conformal coating of nanostructured electrodes.

So far a rather small number of different ALD/MLD precursors have been employed to grow inorganic-organic superlattices. Also, the actual atomic-level structures of these superlattices are not known. The preparation of hybrid inorganic-organic superlattices by means of ALD/MLD is a particularly attractive option for inorganic oxide materials since many oxide materials with exciting properties are composed of abundant elements and are easy to grow with ALD. A prime example of a metal oxide that can be grown with ALD in a highly controllable fashion is ZnO, which has been originally investigated already in the 1980s.^{14, 15} Due to the wide and direct band gap and high piezoelectric efficiency, ZnO is one of the technologically most important oxide materials. Since the ALD fabrication of ZnO thin films is a very well-known process, ZnO does provide a very good platform for proving the benefits of inorganic-organic interface engineering enabled by the ALD/MLD technique. Recently we demonstrated that the ALD/MLD fabrication of hybrid ZnO:hydroquinone (HQ) superlattices indeed yields crystalline superlattice structures with a highly controllable periodicity (Figure 1c, HQ = benzene-1,4-diol, HO-C₆H₄-OH).^{16, 17} The ZnO:HQ superlattices were prepared using diethyl zinc (DEZ) and H₂O as the precursors for ZnO and HQ in the MLD part of the deposition. Crystalline ZnO:HQ superlattice thin films could be prepared with ZnO:HQ ratios varying from 14:1 to 199:1.

So far the structural characteristics of the ZnO:HQ superlattices have not been studied by means of atomistic level simulations and there is little information on their detailed structure-property correlations. Understanding of the atomic-level structure-property correlations would greatly facilitate the systematic improvement of the electronic properties and functionality of the hybrid superlattice materials. Atomistic materials modelling methods enable the systematic investigation of various properties of materials, providing tools for the interpretation, rationalization, and

improvement of experimentally observed characteristics.¹⁸ Furthermore, computational approaches provide very powerful tools for high-throughput screening of potential functional materials.¹⁹ The hybrid nature of inorganic-organic materials adds a new level of complexity to the atomic-level description of the structures, but quantum chemical first-principles approaches are still directly applicable to this new class of materials as long as the methods properly describe both the inorganic and organic parts and the interfaces between them. The present challenges in the *ab initio* modelling of inorganic-organic hybrid materials were recently discussed by Draxl *et al.*²⁰ They focused on solid-state hybrid materials and addressed the question to what extent the hybrid materials can be quantitatively described with *ab initio* methods and where even a qualitative description cannot be reached. The prediction of structural properties, electronic bands, optical excitation spectra, and charge transport in various organic/inorganic interfaces were discussed based on previous literature on computational studies with DFT and many-body perturbation methods.

Here we derive the first atomic-level structural models for the inorganic-organic ZnO:HQ superlattices using quantum chemical methods and carry out detailed first-principles studies to model their structural, spectroscopic, and electronic properties. We moreover compare the theoretical results with our experimental data and provide a detailed interpretation of the experimentally measured infrared spectra, proving the presence of organic interfaces within the ALD/MLD deposited superlattices. The structure-property correlations discovered here provide guidelines for the systematic improvement of the functional properties of the ZnO:HQ superlattices.

Experimental and Computational details

1. ALD/MLD fabrication of the ZnO:HQ superlattices

The ZnO:HQ superlattices were prepared according to the previously reported ALD/MLD process.¹⁶ The Fourier transform infrared spectroscopy (FTIR) measurements reported here were carried out for a ZnO:HQ superlattice sample with a 9:1 ZnO:HQ ratio, where the 9:1 ratio corresponds to the ratio of the ALD and MLD cycles used to deposit ZnO and HQ. X-ray reflection

(XRR) measurements confirm that the periodicity of the ALD/MLD fabricated films varies according to the ZnO:HQ cycle ratio.¹⁶ The 9:1 ZnO:HQ superlattice thin film was deposited on a Si substrate at a deposition temperature of 220°C using an F-120 ALD reactor from ASM Microchemistry Ltd. The precursors used in the deposition were diethylzinc (DEZ) and water (both kept at room temperature) for ZnO layers and HQ (heated to 120 °C) for the organic layers. The deposition consisted of 5 ZnO ALD cycles (DEZ and H₂O, separated by N₂ purges) followed by 60 single MLD cycles of HQ each separated by 9 ALD cycles of ZnO. The final HQ layer was capped with 24 ALD cycles of ZnO to give an ALD/MLD process of 620 total cycles, resulting in a film ca. 100 nm thick.

2. Computational methods

The structures, spectroscopic properties, and electronic properties of the ZnO:HQ superlattices were investigated using the PBE0 hybrid density functional method (DFT-PBE0).^{21, 22} The calculations were carried out with the CRYSTAL14 program package,^{23, 24} utilizing all-electron, Gaussian-type basis sets derived from the molecular Karlsruhe basis sets.²⁵ Two basis sets of different size were applied: larger triple-zeta-valence + polarization (TZVP) level basis set and a smaller split-valence + polarization (SVP) basis (detailed basis set listings are given in the Supporting information). The basis set convergence was also checked with respect to an extended TZVPP basis set (see text for details). The structures and electronic properties of bulk ZnO and all structures based on the ZnO:HQ superlattice **1** were investigated using the TZVP basis set. In the case of the larger ZnO:HQ superlattices **2–4** and the alternative ZnO:HQ superlattice **1b**, the band structures were obtained with single-point TZVP calculations at the SVP-optimized geometries (for comparison, in the case of the ZnO:HQ superlattice **1**, the fully optimized TZVP band gap and single-point TZVP band gap are 1.94 and 2.00 eV, respectively).

In the structural optimizations, both the atomic positions and lattice constants were fully optimized within the constraints imposed by the space group symmetry. The reciprocal space was

sampled using 3x4x1 and 12x12x8 Monkhorst-Pack-type k -point grids for ZnO:HQ superlattices and bulk ZnO, respectively (convergence tests with denser 6x6x1 mesh for the ZnO:HQ superlattices showed negligible energy difference to the applied 3x4x1 mesh)²⁶. For the evaluation of the Coulomb and exchange integrals (TOLINTEG), tight tolerance factors of 8, 8, 8, 8, and 16 were used. The fully optimized ZnO:HQ superlattices showed cell angles of 87–90° and an energy comparison with structures optimized while imposing a constraint of 90° cell angles resulted in an energy loss of 0.2 kJ/mol per atom. Since the analysis of the properties of the materials is much more practical for orthogonal unit cells in comparison to non-orthogonal ones, the cell angles of all ZnO:HQ superlattices were fixed to 90°. Default optimization convergence thresholds were applied in structural optimizations and default numerical integration grid (XLGRID) was used for the integration of the exchange-correlation functional.

The Gamma-point harmonic vibrational frequencies were obtained by using the computational scheme implemented in CRYSTAL^{27, 28} and the infrared (IR) and Raman intensities were calculated using the analytical coupled perturbed Hartree-Fock/Kohn-Sham method.^{29, 30} The spectroscopic properties were investigated using the SVP basis set. The predicted IR and Raman spectra are based on the harmonic approximation and the wavenumbers have been scaled by a factor of 0.95 to account for the overestimation typical for *ab initio* harmonic frequencies.^{31, 32} The IR absorbance spectrum is a superposition of Lorentzian peak shapes with FWHM of 32 cm⁻¹. The Raman intensities have been calculated for a polycrystalline powder sample (total isotropic intensity in arbitrary units). The final spectrum was obtained by using pseudo-Voigt peak profile (50:50 Lorentzian:Gaussian) and FWHM of 32 cm⁻¹. The reciprocal space k -paths used in the band structure analysis were taken from Setyawan and Curtarolo.³³ The structural figures were prepared using the VESTA visualization program.³⁴

Results and Discussion

1. Structural Properties

We investigated the structural and electronic properties of bulk ZnO and ZnO:HQ superlattices using the PBE0 hybrid density functional method (see Experimental section for details). Hybrid density functional methods have been recently benchmarked and successfully applied in several computational investigations on hybrid ZnO/organic materials and interfaces.³⁵⁻³⁸

We derived explicit atomistic structural models for the ZnO:HQ superlattices starting from bulk ZnO. Bulk ZnO crystallizes in the hexagonal wurtzite structure with four atoms in the primitive cell (space group $P6_3mc$). The lattice parameters predicted with the DFT-PBE0 method are in very good agreement with the experimental values for bulk ZnO ($a = 3.250 \text{ \AA}$ and $c = 5.207 \text{ \AA}$).³⁹ The difference between the experimental and calculated lattice parameters a/c is $+0.5\%/+0.1\%$ for the larger TZVP basis set and $+0.1\%/-0.4\%$ for the smaller SVP basis set. For creating atomic-level models of the ZnO:HQ superlattices, we first had to consider the preferred orientation of ZnO in the ALD/MLD grown superlattices. From the large number of experimental studies, it is known that ZnO thin films can be grown with both [100] and [002] orientation,¹⁵ the preferred orientation being dependent for example on the deposition temperature. In the case of the hybrid ZnO:HQ superlattices prepared so far, the deposition temperature was set to 220°C ,¹⁶ and based on previous experimental evidence, the [100] direction should still be the preferred growth direction for temperatures up to around 220°C , the [002] direction becoming the favored growth direction when the deposition temperature is further increased.

Considering the experimental evidence on the preferred growth direction of ZnO, we chose to derive atomic level models for the ZnO:HQ superlattices in the [100] growth direction. The effect of the temperature on the preferred growth direction of the ZnO:HQ superlattices is currently being investigated both experimentally and theoretically and will be addressed in future studies. It should be noted that cleaving bulk ZnO perpendicular to the [002] growth direction results polar surfaces, which must be dealt with very carefully in computational studies due to the electrostatic instabilities

arising from such surfaces.⁴⁰ Cleaving bulk ZnO perpendicular to the [100] growth direction results in non-polar surfaces that are less complicated to deal with.⁴¹

After choosing the orientation of the ZnO part of the ZnO:HQ superlattices, we considered the structure of the ZnO:HQ interface. A key question for deriving the ZnO:HQ interface structure is the density of the molecular HQ layer with respect to the ZnO(100) surface ($a = 3.25 \text{ \AA}$ and $b = 5.21 \text{ \AA}$ for the surface unit cell). In principle, every surface Zn-site could bond one HQ molecule via Zn–O bond. However, as shown in Figure 2a, applying such 1x1 surface coverage leads to very crowded ZnO:HQ interface: the shortest distance between the HQ molecules in the a direction is only 2.9 \AA , implying clearly repulsive interactions between the HQ molecules.⁴² In the 1x1 model, the surface O-sites would be saturated with hydrogen atoms.

Doubling the lattice vector a and introducing HQ molecules only on 50% of the surface Zn-sites results in a more reasonable 2x1 surface coverage (Figure 2b). Here, the other 50% of the surface Zn-sites are saturated with OH groups and all O-sites are saturated with H atoms. When surface is relaxed by means of an unconstrained geometry optimization, the Zn–OH species attract a proton from the neighboring surface O-site, resulting in the formation of H₂O molecules on the surface Zn-sites. The H₂O molecule remains strongly hydrogen bonded with the neighboring surface O-site. Half of the H-saturated surface O-sites must remain protonated as the neighboring surface Zn-site is bound to a HQ molecule and cannot attract the proton from the surface O-site. These surface OH species are hydrogen bonded with the O atoms of the neighboring HQ molecules.

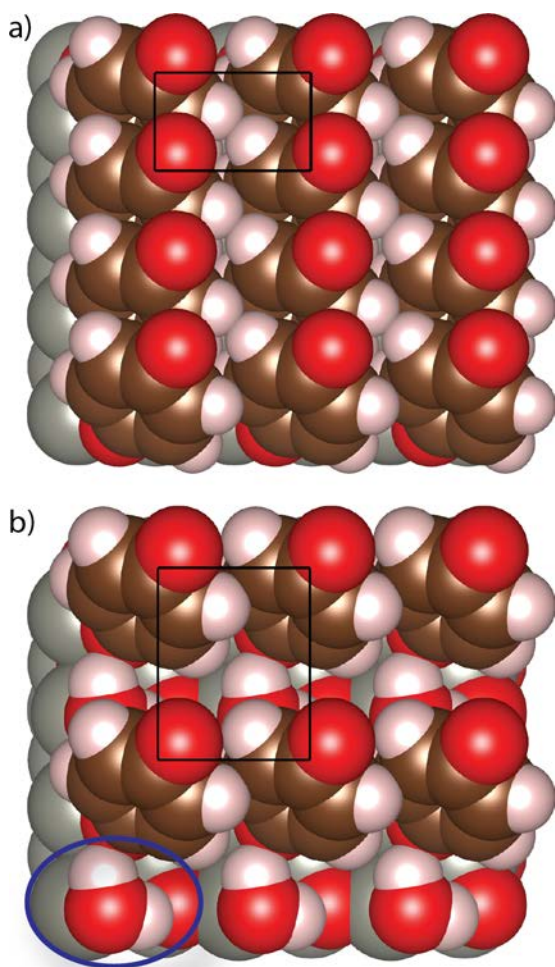


Figure 2. Two different surface coverage models for a HQ-covered ZnO(100) surface (space-filling representation). The surfaces shown here have been cleaved from optimized ZnO:HQ superlattice structures, the unit cell is denoted with black lines. a) 1x1 model with HQ molecule at every surface Zn-site and surface O-site saturated with hydrogen atoms ($a = 3.25 \text{ \AA}$; $b = 5.21 \text{ \AA}$). b) 2x1 model with HQ molecules at 50% of surface Zn-sites, OH at the other 50% of surface Zn-sites and surface O-sites saturated with hydrogen atoms ($a = 6.50 \text{ \AA}$; $b = 5.21 \text{ \AA}$). In the model b), an example of the H₂O molecules forming at the OH-terminated Zn-sites during the geometry optimization is highlighted in blue. The coloring scheme is as follows: gray = Zn, red = O, brown = C, white = H.

In the 2x1 surface coverage model illustrated in Figure 2b, the HQ molecules are arranged in a striped pattern. To further check the effect of the surface coverage model, we investigated an alternative checkerboard-type bonding pattern for the HQ molecules. In this model, the total HQ coverage of the Zn-sites is identical to the striped model (50%), but after doubling the lattice vector b the HQ molecules can be arranged in a checkerboard-type pattern (see Supporting information.

for an illustration of the model). Similar checkerboard-type pattern has been recently applied by Hofmann *et al.* when studying the adsorption of pyridine on the ZnO(100) surface.³⁸ A comparison of the total energies of the striped and checkerboard-type models shows that the energy difference of the models is less than 0.1 kJ/mol per atom, which is an insignificant difference considering the level of theory applied here. The coverage models are thus practically isoenergetic and the rest of our calculations have been carried out using the striped model illustrated in Figure 2b. However, we have also investigated the effect of the surface coverage model on the electronic properties of the ZnO:HQ superlattices (see section 3 below).

Similar to the striped surface coverage model, the geometry optimization of the checkerboard-type model results in the formation of H₂O molecules on all surface Zn-sites which are not bound to a HQ molecule. Also here 50% of the H-saturated surface O-sites must remain protonated as the neighboring surface Zn-site is bound to a HQ molecule and cannot attract the proton from the surface O-site. The transformation of the Zn–OH surface species into H₂O molecules is also in line with the previous experimental and theoretical evidence of the behavior of water on defect-free ZnO(100) surfaces.^{43, 44} These studies have shown that adsorption of water on ZnO(100) leads to the partial dissociation of water molecules, giving rise to a well-defined 2x1 superstructure. The studied ZnO:HQ superlattices actually show the same 2x1 superstructure for surface O-sites: 50% of the O-sites are hydrogen-bonded to the neighboring Zn–H₂O surface species and 50% of the O-sites remain protonated and form a hydrogen-bond with the neighboring Zn–HQ surface species.

After choosing the 50% density for the HQ interface with respect to the surface Zn sites, we systematically investigated the eight different Zn–HQ–Zn bonding schemes that arise at the ZnO:HQ interface for the present superlattice models. In these comparisons we considered a ZnO:HQ superlattice that has a ZnO slab of 1.2 nm between the HQ interlayers (Figure 3). The energetically most favorable Zn–HQ–Zn bonding scheme, illustrated in Figure 3, turned out to be 27 kJ/mol lower in energy than the second most favorable scheme. We have applied the energetically most favorable bonding scheme for all studied ZnO:HQ superlattices, while the

description of the other investigated bonding schemes can be found from the Supporting information. From now on, the ZnO:HQ superlattice structure with a ZnO slab of 1.2 nm between the HQ interlayers is denoted as superlattice **1**. In addition to this superlattice, we investigated three larger superlattices **2–4** having ZnO slab thicknesses of 2.6, 5.5, and 11.0 nm, respectively. The largest studied superlattice **4** is also shown in Figure 3. The number of atoms in the primitive unit cell is 60, 100, 180, and 340 for the superlattice structures **1–4**, respectively (space group *P1*). A geometry optimization of the superlattice **1** using both TZVP and SVP level basis sets shows that the geometry of the superlattice is rather well converged already with the smaller SVP level basis set. The lattice parameters *a*, *b*, and *c* predicted using the TZVP basis set are 0.3%, 0.6%, and 0.4% larger than with the SVP basis set.

Considering the ZnO:HQ superlattices experimentally prepared with ALD/MLD, the ratio of ZnO and HQ deposition cycles has been varied from 199:1 to 1:1.¹⁶ The deposited superlattices show good crystallinity at least down to ZnO:HQ ratios of 14:1. The thickness of the ZnO slab in the largest superlattice structure **4** studied here (11 nm) is in fact intermediate between the ZnO block thicknesses measured for the 74:1 (12 nm) and 59:1 (9.7 nm) ZnO:HQ superlattices.¹⁷

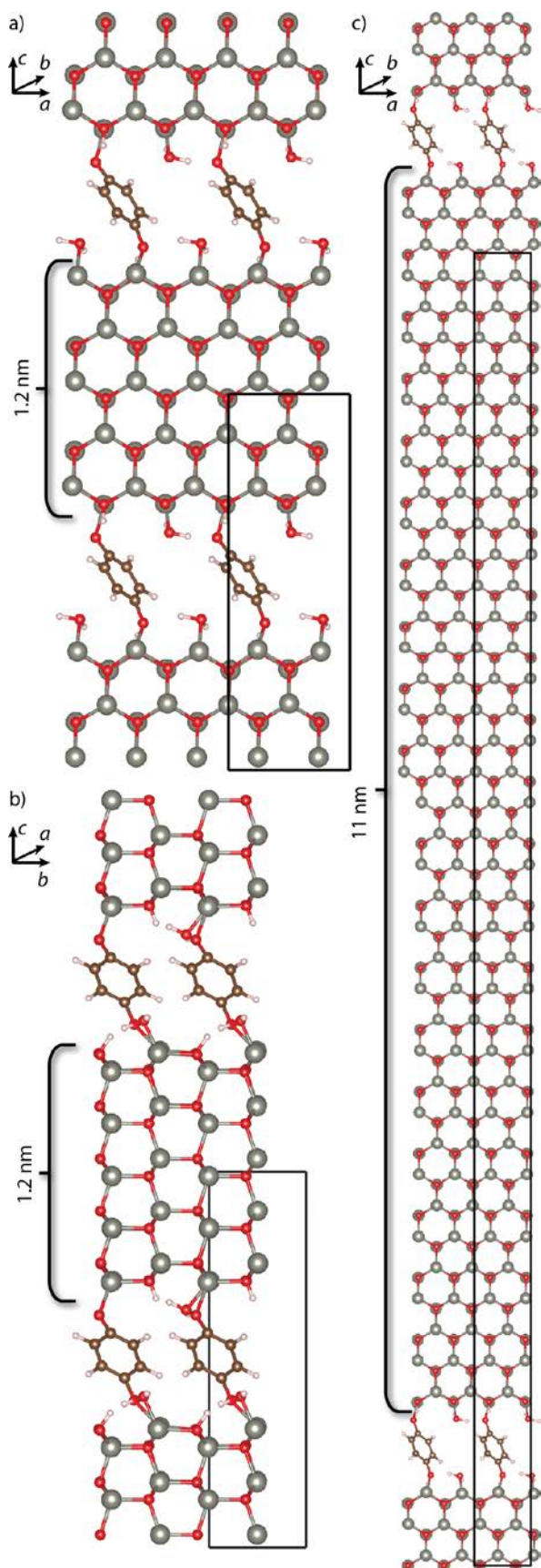


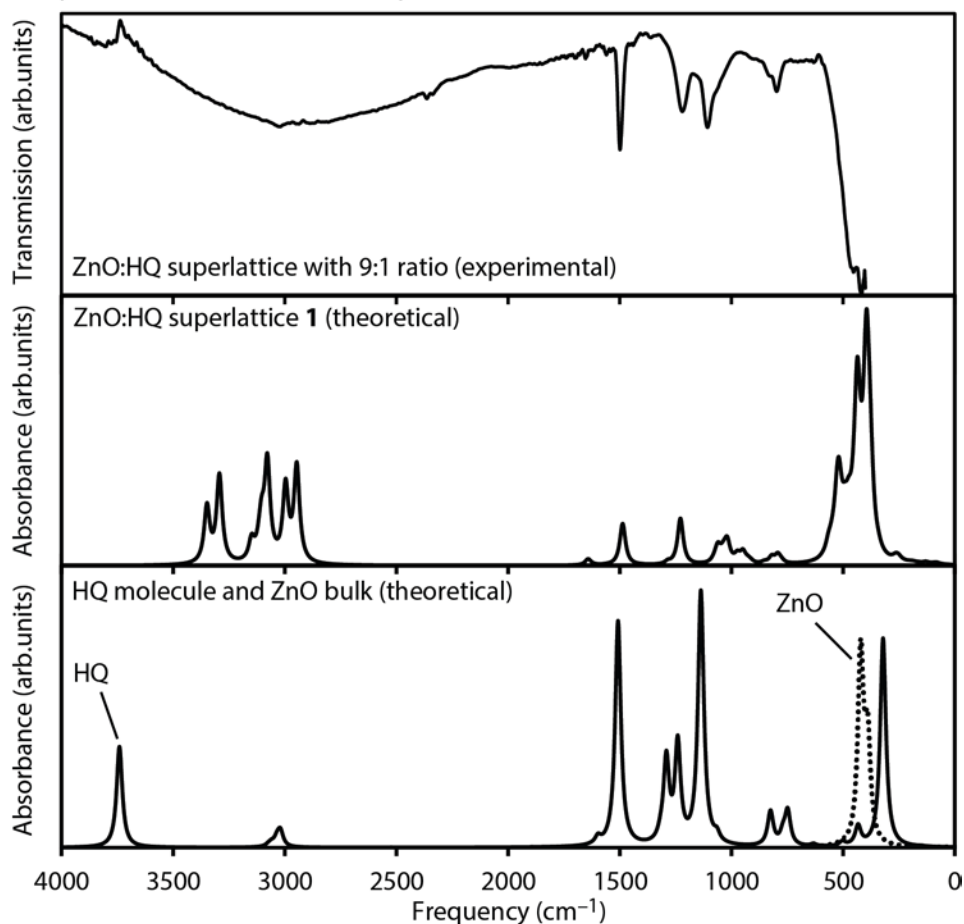
Figure 3. Optimized structures of two different ZnO:HQ superlattices (unit cell denoted with black lines). a) ZnO:HQ superlattice **1** viewed along the b axis. b) ZnO:HQ superlattice **1** along the a axis. c) ZnO:HQ superlattice **4** viewed along the b axis.

2. Spectroscopic Properties

We carried out harmonic frequency calculations for the ZnO:HQ superlattices **1** and **2** to confirm that the optimized structures are true local minima. For the superlattice **1**, we also calculated the IR and Raman spectra, which are shown in Figure 4 together with an experimental IR spectrum for a ZnO:HQ superlattice deposited with ZnO:HQ ratio of 9:1 (see Experimental section for details on the fabrication of the superlattice). Based on the ZnO growth rates observed during the ALD process (1.65 Å per cycle),¹⁵ the HQ interlayer spacing in the ZnO:HQ superlattice **1** (1.2 nm) is of the same magnitude as for the experimental 9:1 superlattice (ca. 1.5 nm).

Comparison between the predicted and experimental IR spectrum shows that the important features of the ZnO:HQ superlattices are reproduced well by the theoretical spectrum.¹⁶ In the experimental spectrum, a very broad mode centred at about 3000 cm⁻¹ is observed in the high frequency range (> 2000 cm⁻¹). Detailed theoretical analysis of the vibrational modes shows that the high-frequency peaks arise from O–H stretching modes of the OH and H₂O surface species at the ZnO:HQ interface. The highest energy modes at 3350–3300 cm⁻¹ are due to surface OH species (surface O-sites saturated with H atoms that are hydrogen bonded to an O atom of a neighboring HQ molecule). The O–H stretching frequencies due to surface H₂O species are split in two sets: 3100–3080 cm⁻¹ and 3000–2950 cm⁻¹. The former modes arise from O–H bonds where the H atom is hydrogen bonded to an O atom of a HQ molecule, while the latter modes are due to O–H bonds where the H atom is hydrogen bonded to a surface O-site. The energy ordering of the modes also suggests that the hydrogen bond between the surface H₂O species and the free surface O-site is stronger than the hydrogen bond between the surface H₂O species and the HQ molecule.

a) Experimental and theoretical IR spectra



b) Theoretical Raman spectra

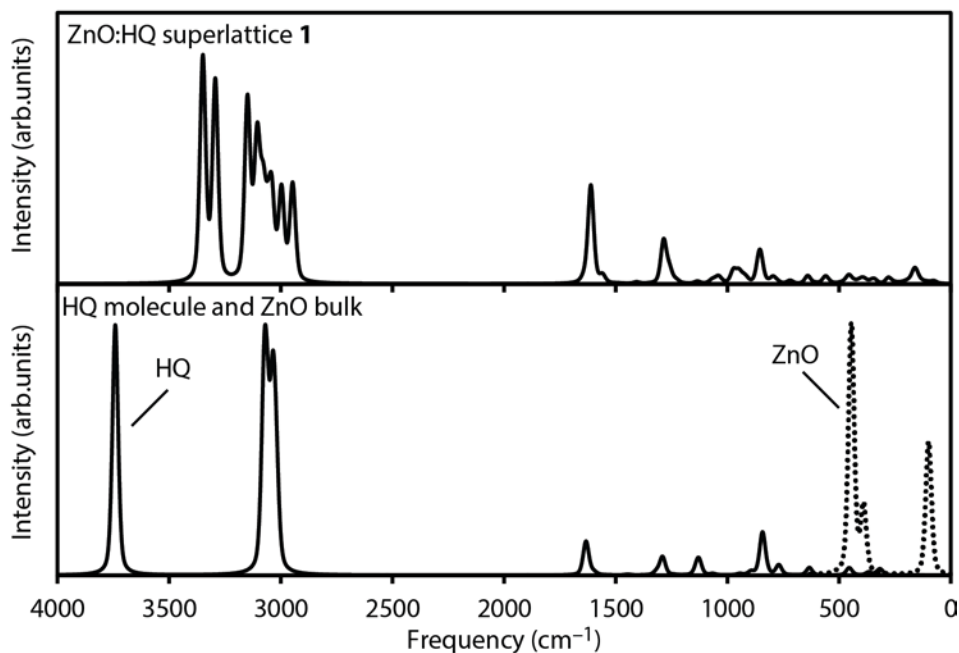


Figure 4. a) Experimental and theoretical IR spectra for ZnO:HQ superlattice with ratio 9:1, ZnO:HQ superlattice 1, HQ molecule and ZnO bulk. b) Theoretical Raman spectra for the ZnO:HQ superlattice 1, HQ molecule, and bulk ZnO.

The IR spectrum of the free HQ molecule shows an O–H stretching mode at 3739 cm^{-1} and a C–H stretching mode at 3020 cm^{-1} . The O–H stretching mode obviously cannot exist in the predicted IR spectrum of the ZnO:HQ superlattice **1** since the OH group of the HQ molecule has already reacted with Zn. Comparison with the experimental IR spectrum suggests that no unreacted OH groups of the HQ molecule should remain in the ZnO:HQ superlattice. The C–H stretching modes of the HQ molecule are located at $3115\text{--}3040\text{ cm}^{-1}$ in the ZnO:HQ superlattice, but due to their low intensity they are overlapped by the O–H stretching features.

Perhaps the most important fingerprint mode in the IR spectrum of the ZnO:HQ superlattices indicating the presence of the HQ interlayers is the aromatic C=C stretching mode. This mode can be found at 1507 , 1490 , and 1500 cm^{-1} for the free HQ molecule, ZnO:HQ superlattice **1**, and experimental ZnO:HQ (9:1) superlattice, respectively. The narrow peak is very clearly visible in all three spectra. In the case of the ZnO:HQ superlattice **1**, the very weak mode at 1643 cm^{-1} arises from the H–O–H scissoring mode of the surface H_2O species. In the case of the free HQ molecule, the next mode at 1292 cm^{-1} arises from in-plane C–H bending, but this mode becomes very weak in the superlattice structure and cannot be seen in the theoretical or experimental spectrum of the ZnO:HQ superlattice. Another important fingerprint mode for the HQ molecule is the C–O stretching mode coupled with C-H in-plane bending, which can be clearly seen at 1237 , 1230 , and 1220 cm^{-1} for the free HQ molecule, ZnO:HQ superlattice **1**, and experimental ZnO:HQ (9:1) superlattice, respectively.

When moving to lower frequencies after the fingerprint modes at about 1500 and 1220 cm^{-1} , the three spectra show clear differences. In the spectrum of the free HQ molecule, the next mode at 1136 cm^{-1} is actually the most intensive one, but it is not present at all in the spectrum of the ZnO:HQ superlattice **1**. In the free molecule this mode arises from the in-plane O–H bending of the OH group of the HQ molecule, and this functional group is no longer present in the superlattice structure after the HQ molecule has reacted with Zn. The experimental spectrum does show a peak at 1105 cm^{-1} , but this peak is in fact due to the silicon substrate used in the deposition of the

ZnO:HQ superlattice.¹⁶ Moving further to the lower frequencies, the ZnO:HQ superlattice **1** shows several small features at 1059–950 cm^{-1} , which are not present in the spectrum of the free HQ molecule. These modes are due to rocking and wagging modes of H atoms of the surface H_2O and OH species and the 1105 cm^{-1} peak arising from the Si substrate in the experimental IR spectrum does also possess a shoulder between 1050–1000 cm^{-1} .

All three spectra show one more HQ fingerprint mode due to C–H out-of-plane bending at 827, 820–800, and 830–800 cm^{-1} for the free HQ molecule, ZnO:HQ superlattice **1**, and experimental ZnO:HQ (9:1) superlattice, respectively. The peak located at 740 cm^{-1} in the spectrum of the free HQ molecule is not visible in the superlattice spectra, it is due to a C=C/C–O stretching mode with no coupling to C–H bending. Finally, the ZnO modes become active in the low-frequency range starting from 600 cm^{-1} . The strong peak at 433 cm^{-1} in the spectrum of the free HQ molecule is due to C–O in-plane bending and it is not active in the ZnO:HQ superlattice where the HQ molecule has formed covalent bonds with Zn atoms. Comparison with the IR spectrum of bulk ZnO shows that some ZnO modes are shifted to higher energies in the theoretical and experimental IR spectrum of the ZnO:HQ superlattice. In the case of bulk ZnO, the onset of the modes is at about 500 cm^{-1} , while for the ZnO:HQ superlattice the highest energy ZnO modes become active already at about 600 cm^{-1} because of the non-bulk Zn–O bonding at the ZnO:HQ interfaces.

In the case of the Raman spectrum, we currently have no experimental data available for comparison. At high frequencies, the predicted Raman spectra can be described in almost similar fashion to the IR spectra. The high-frequency O–H stretching mode of the free HQ molecule (3739 cm^{-1}) disappears in the superlattice spectrum, while new strong high-frequency modes arise between 3400–2900 cm^{-1} due to the O–H stretching modes of the surface OH and H_2O species. The C–H stretching modes of the HQ molecule at 3100–3000 cm^{-1} are much more intensive in the Raman spectrum in comparison to the IR spectrum and they are present also in the superlattice spectrum (mixed in with the OH stretching features).

The most important features in the predicted spectrum are the strong 1610 cm^{-1} aromatic C=C stretch and 1280 cm^{-1} C–O stretch, which should be very good fingerprint modes for confirming the presence of the HQ molecules in the experimental Raman spectra of ZnO:HQ superlattices. These fingerprint modes are slightly different from the IR fingerprint modes at about 1500 and 1220 cm^{-1} : for the IR modes, the C=C stretching and C–O stretching are clearly coupled with C–H in-plane bending, but for the Raman fingerprint modes there is no such coupling. Thus the IR and Raman fingerprint modes might change in rather different ways if the organic building block of the ZnO:organic superlattice is modified via aromatic substitution.

In contrast to the theoretical IR spectrum, the bulk-like ZnO modes occurring at frequencies smaller than 600 cm^{-1} show only small intensities in the predicted Raman spectrum of the ZnO:HQ superlattice **1**. The Raman intensities shown in Figure 4 have been predicted for a polycrystalline sample and for a single-crystalline sample the intensities would be direction-dependent. At least for the polycrystalline case, the Raman spectrum of the ZnO:HQ superlattice **1** appears to be dominated by the modes arising from the organic parts of the superlattice.

3. Electronic Properties and Band Structure Engineering

We also investigated the fundamental electronic properties of the ZnO:HQ superlattices to understand the effects of introducing the inorganic-organic interfaces to ZnO. From a computational point of view, it is important to note that the standard DFT-GGA functionals such as PBE clearly underestimate the band gap of ZnO, typically predicting $E_{\text{gap}} = 0.9\text{ eV}$ in comparison to the experimental 0 K estimate of 3.44 eV .^{45, 46} This issue can be corrected by applying Hubbard-like corrections (PBE+U) or by applying hybrid density functionals where no semi-empirical corrections are necessary. Since we use the hybrid DFT-PBE0 functional, the band structure and band gap predicted for bulk ZnO are in very reasonable agreement with the experiment. The direct band gap of bulk ZnO is predicted to be 3.81 , 3.55 , and 3.53 eV at the PBE0/SVP, PBE0/TZVP, and PBE0/TZVPP levels of theory, respectively. The result obtained using the TZVP basis set is already

rather well-converged with respect to the extended and computationally much more expensive TZVPP basis set. The PBE0/TZVP band gap of 3.55 eV also compares well with the experimental 0 K estimate of 3.44 eV.⁴⁶ Concerning previous computational studies on ZnO, PBE0 band gaps of 3.32 and 3.2 eV have been predicted using full-potential linearized augmented-planewave (FLAPW) and projector-augmented-wave (PAW) basis sets, respectively.⁴⁷⁻⁵⁰

The band structure of bulk ZnO calculated at the PBE0/TZVP level of theory is shown in Figure 5a and a comparison to the band structures calculated with the SVP and TZVPP level basis sets is shown in Supporting information. Figure 5 also shows the band-projected electron densities for the highest valence band (VB) and the lowest conduction band (CB). In the case of bulk ZnO, it is clear that both VB and CB shown in Figure 5 are highly delocalized over the whole structure, possessing O and mixed O–Zn character, respectively.

Comparison of the band structure of the ZnO:HQ superlattice **1** in Figure 5b to the band structure of bulk ZnO reveals interesting differences. The pseudo band-gap originating from the ZnO part of the structure now has two rather flat bands in it, which decrease the band gap of the ZnO:HQ superlattice **1** to 1.94 eV. Furthermore, the band gap is no longer direct. The origin of these molecular-type bands immediately becomes clear by inspection of the band-projected electron densities: The VB is dominated by contributions from the organic HQ molecules and by running a molecular calculation on isolated HQ, we could confirm that the HOMO of HQ is indeed located within the energy gap of ZnO. In contrast to the VB, the CB is a delocalized band dominated by contributions from ZnO, showing just some minor contributions from the HQ molecule. We also checked the effect of alternative HQ bonding pattern on the ZnO surface by calculating the band structure of the checkerboard-type bonding pattern of HQ molecules (ZnO:HQ superlattice **1b**, see Supporting information). The band gap remains indirect also for the checkerboard-type bonding pattern, but the obtained band gap of 2.10 eV is slightly larger than for the superlattice **1**.

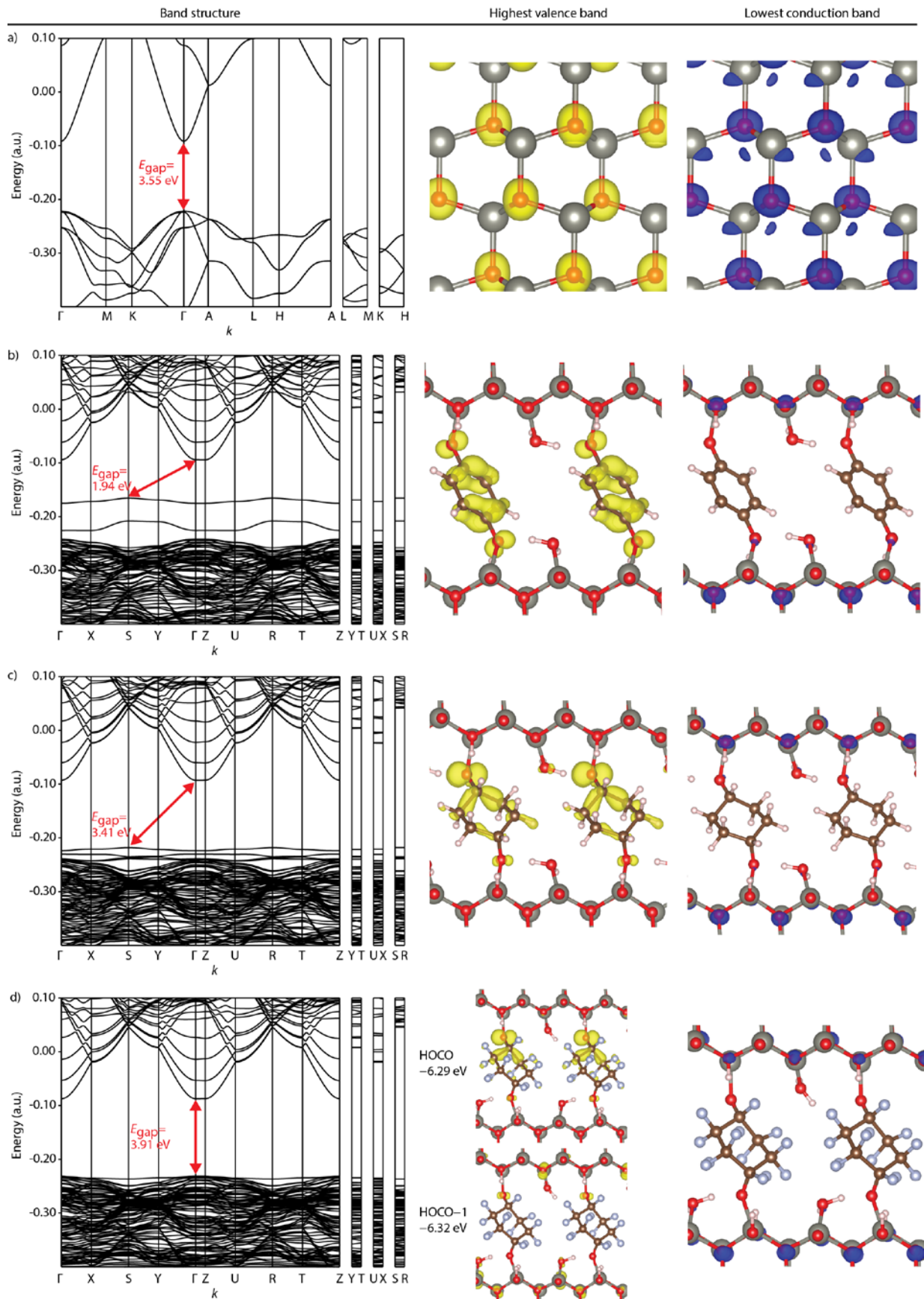


Figure 5. Band structures, band gaps, and band-projected electron densities for a) ZnO, b) ZnO:HQ superlattice **1**, c) saturated modification of **1**, and d) saturated + fluorinated modification of **1** (showing the two highest energy valence bands HOCO and HOCO-1) Density isovalues: 0.01 and 0.002 a.u. for VB and CB in ZnO:HQ superlattices, 0.02 and 0.01 a.u. in ZnO.

Considering the notable effect of the HQ molecule on the band structure of the ZnO:HQ superlattice **1**, we investigated several hypothetical modifications of **1**, where we used other organic molecules than HQ. First, we substituted the four hydrogen atoms in the aromatic ring of the HQ molecule with electron-withdrawing fluorine atoms. This resulted in a clearly increased band gap from 1.94 eV to 2.32 eV. Substituting the hydrogen atoms with electron-donating amine groups (NH₂) shows a consistent effect in the other direction, the band gap decreasing from 1.94 eV to 1.70 eV. After these preliminary tests we carried out a more detailed investigation for ZnO:organic superlattices where the organic molecule is the saturated analogue of HQ, i.e. 1,4-cyclohexanediol (CHD). The band structure and band-projected electron densities of the ZnO:CHD superlattice are shown in Figure 5c. Replacing the aromatic HQ molecules with the saturated CHD molecules changes the energy levels of the organic interface significantly, resulting in a band gap of 3.41 eV. However, the band gap remains indirect similar to the superlattice **1** and the highest valence band is a localized band arising from the CHD molecules. To push the energy levels of the organic part further down, we replaced the hydrogen atoms in the CHD ring with fluorine atoms. The band structure and band-projected electron densities of the resultant ZnO:CHDF superlattice are illustrated in Figure 5d, showing how this modification brings the highest-energy band of the organic part to the level of the topmost ZnO valence bands. The band gap increases to 3.91 eV and becomes direct as in bulk ZnO. Inspection of the band-projected electron densities reveals that the highest occupied crystal orbital (HOCO) is still a localized molecular band, while the second highest HOCO-1 band lying only 0.03 eV below HOCO at the Γ point is a ZnO-type delocalized band. The valence maximum of the molecular band has thus shifted from the S point to the Γ point. The overall message from the band structures illustrated in Figure 5 is that by changing the organic molecule in the ZnO:organic superlattices, the magnitude of the band gap can be tuned rather flexibly. Obtaining direct band gap superlattices is a more challenging task, but the most straightforward way towards such materials might be to focus on organic molecules having HOMO energies clearly lower than the ZnO valence bands.

The band gap of ZnO:CHDF is even larger than for bulk ZnO (3.91 vs 3.55 eV) due to well-known quantum confinement effects arising from the nanostructuring: the band gap of the nanosized ZnO layers is higher than that of bulk ZnO. The role of the quantum confinement is confirmed by comparing the band gaps of all the four ZnO:HQ superlattices **1–4**: the band gaps are 1.94, 1.79, 1.73, and 1.69 eV, respectively. Hence, the pseudo ZnO band gap of the ZnO:HQ superlattice decreases with increasing thickness of the ZnO block, the decrease being mainly due to the shifting of the lowest CB. Similar quantum confinement effect has been recently reported for ZnO surfaces and nanowires by Dominguez *et al.*⁵⁰ The band structures of the ZnO:HQ superlattices **2–4** are given in Supporting Information.

The trend in basic electronic properties illustrated in Figure 5 suggests that the transport properties of the ZnO:organic superlattices could be tailored by the choice of the organic constituent. Experimentally, the key question is whether we can develop a feasible ALD/MLD process for the selected inorganic:organic superlattice composition. The first criterion is whether we can find a suitable deposition temperature. For 1,4-cyclohexanediol the melting and boiling points are 98 and 150 °C, respectively, being lower than those for HQ (172 and 285 °C), Hence it is important to note that crystalline ZnO thin films can be grown in a wide temperature range, and at temperatures considerably lower than the deposition temperature employed for the present ZnO:HQ superlattices.⁵¹

Conclusions

We first derived atomic-level structural models by quantum chemical methods for inorganic-organic ZnO:HQ superlattices fabricated through alternating atomic and molecular layer deposition (ALD/MLD) cycles. Then through a first-principles study the structural, spectroscopic and electronic properties of these superlattice structures were investigated. In particular, we were able to perfectly interpret the infrared spectra measured for these materials to prove the presence of organic interfaces within the crystalline ZnO matrix. Then, most excitingly we demonstrated with several

illustrative examples how the band structure of the superlattice could be engineered in an experimentally feasible way by making small modifications in the organic constituent. We foresee that our atomic-level approach to model the ALD/MLD hybrid materials and the guidelines revealed thereof for the band-structure engineering are an important step ahead towards the rational design and tailoring of these unique hybrid materials for novel material functionalities and/or enhanced performance.

Supporting Information Available: Additional computational details, supplementary computational results, and unit cell coordinates of the studied structures. This material is available free of charge via the Internet at <http://pubs.acs.org>.

Acknowledgements

The present work has received funding from the European Research Council under the European Union's Seventh Framework Programme (FP/2007–2013)/ERC Advanced Grant Agreement (no. 339478) and the Aalto Energy Efficiency Research Programme. A. J. K. gratefully acknowledges funding from the Alfred Kordelin Foundation and the Foundation for Research of Natural Resources in Finland. The Finnish IT Center for Science (CSC) is thanked for providing the computing resources for this work.

References

- (1) George, S. M. Atomic Layer Deposition: An Overview. *Chem. Rev.* **2010**, *110*, 111-131.
- (2) Miikkulainen, V.; Leskelä, M.; Ritala, M.; Puurunen, R. L. Crystallinity of Inorganic Films Grown by Atomic Layer Deposition: Overview and General Trends. *J. Appl. Phys.* **2013**, *113*, 021301/1-021301/101.
- (3) Pinna, N.; Knez, M., Eds.; *Atomic Layer Deposition of Nanostructured Materials*; Atomic Layer Deposition of Nanostructured Materials, Wiley-VCH: Weinheim, 2012.
- (4) Dameron, A. A.; Seghete, D.; Burton, B. B.; Davidson, S. D.; Cavanagh, A. S.; Bertrand, J. A.; George, S. M. Molecular Layer Deposition of Alucone Polymer Films using Trimethylaluminum and Ethylene Glycol. *Chem. Mater.* **2008**, *20*, 3315-3326.

- (5) Peng, Q.; Gong, B.; VanGundy, R. M.; Parsons, G. N. "Zincone" Zinc Oxide - Organic Hybrid Polymer Thin Films Formed by Molecular Layer Deposition. *Chem. Mater.* **2009**, *21*, 820-830.
- (6) Klepper, K. B.; Nilsen, O.; Fjellvåg, H. Deposition of Thin Films of Organic-Inorganic Hybrid Materials Based on Aromatic Carboxylic Acids by Atomic Layer Deposition. *Dalton Trans.* **2010**, *39*, 11628-11635.
- (7) Sood, A.; Sundberg, P.; Malm, J.; Karppinen, M. Layer-by-Layer Deposition of Ti-4,4'-Oxydianiline Hybrid Thin Films. *Appl. Surf. Sci.* **2011**, *257*, 6435-6439.
- (8) Sundberg, P.; Karppinen, M. Organic and Inorganic-Organic Thin Film Structures by Molecular Layer Deposition: A Review. *Beilstein J. Nanotechnol.* **2014**, *5*, 1104-1136.
- (9) Sundberg, P.; Karppinen, M. Organic-Inorganic Thin Films from TiCl₄ and 4-Aminophenol Precursors: A Model Case of ALD/MLD Hybrid-Material Growth? *Eur. J. Inorg. Chem* **2014**, 968-974.
- (10) Costescu, R. M.; Cahill, D. G.; Fabreguette, F. H.; Sechrist, Z. A.; George, S. M. Ultra-Low Thermal Conductivity in W/Al₂O₃ Nanolaminates. *Science* **2004**, *303*, 989-990.
- (11) Tynell, T.; Giri, A.; Gaskins, J.; Hopkins, P. E.; Mele, P.; Miyazaki, K.; Karppinen, M. Efficiently Suppressed Thermal Conductivity in ZnO Thin Films Via Periodic Introduction of Organic Layers. *J. Mater. Chem. A* **2014**, *2*, 12150-12152.
- (12) Ohta, H.; Kim, S.; Mune, Y.; Mizoguchi, T.; Nomura, K.; Ohta, S.; Nomura, T.; Nakanishi, Y.; Ikuhara, Y.; Hirano, M.; Hosono, H.; Koumoto, K. Giant Thermoelectric Seebeck Coefficient of a Two-Dimensional Electron Gas in SrTiO₃. *Nat. Mater.* **2007**, *6*, 129-134.
- (13) Niemelä, J. P.; Karppinen, M. Tunable Optical Properties of Hybrid Inorganic-Organic [(TiO₂)_m(Ti-O-C₆H₄-O-)_k]_n Superlattice Thin Films. *Dalton Trans.* **2014**, *44*, 591-597.
- (14) Tammenmaa, M.; Koskinen, T.; Hiltunen, L.; Niinistö, L.; Leskelä, M. Zinc Chalcogenide Thin Films Grown by the Atomic Layer Epitaxy Technique using Zinc Acetate as Source Material. *Thin Solid Films* **1985**, *124*, 125-128.
- (15) Tynell, T.; Karppinen, M. Atomic Layer Deposition of ZnO: A Review. *Semicond. Sci. Technol.* **2014**, *29*, 043001/1-043001/15.
- (16) Tynell, T.; Karppinen, M. ZnO:Hydroquinone Superlattice Structures Fabricated by atomic/molecular Layer Deposition. *Thin Solid Films* **2014**, *551*, 23-26.
- (17) Tynell, T.; Yamauchi, H.; Karppinen, M. Hybrid Inorganic-Organic Superlattice Structures with Atomic Layer deposition/molecular Layer Deposition. *J. Vac. Sci. Technol. A* **2014**, *32*, 01A105/1-01A105/5.
- (18) Carter, E. A. Challenges in Modeling Materials Properties without Experimental Input. *Science* **2008**, *321*, 800-803.
- (19) Curtarolo, S.; Hart, G. L. W.; Nardelli, M. B.; Mingo, N.; Sanvito, S.; Levy, O. The High-Throughput Highway to Computational Materials Design. *Nat. Mater.* **2013**, *12*, 191-201.
- (20) Draxl, C.; Nabok, D.; Hannewald, K. Organic/inorganic Hybrid Materials: Challenges for Ab Initio Methodology. *Acc. Chem. Res.* **2014**, *47*, 3225-3232.

- (21) Perdew, J. P.; Burke, K.; Ernzerhof, M. Generalized Gradient Approximation made Simple. *Phys. Rev. Lett.* **1996**, *77*, 3865-3868.
- (22) Adamo, C.; Barone, V. Toward Reliable Density Functional Methods without Adjustable Parameters: The PBE0 Model. *J. Chem. Phys.* **1999**, *110*, 6158-6170.
- (23) Dovesi, R.; Orlando, R.; Erba, A.; Zicovich-Wilson, C. M.; Civalleri, B.; Casassa, S.; Maschio, L.; Ferrabone, M.; De La Pierre, M.; D'Arco, P.; Noël, Y.; Causà, M.; Rérat, M.; Kirtman, B. CRYSTAL14: A Program for the Ab Initio Investigation of Crystalline Solids. *Int. J. Quant. Chem.* **2014**, *114*, 1287-1317.
- (24) Dovesi, R.; Saunders, V. R.; Roetti, C.; Orlando, R.; Zicovich-Wilson, C. M.; Pascale, F.; Civalleri, B.; Doll, K.; Harrison, N. M.; Bush, I. J.; D'Arco, P.; Llunell, M.; Causà, M.; Noël, Y., *CRYSTAL14 User's Manual. University of Torino: Torino, Italy, 2014.*
- (25) Weigend, F.; Ahlrichs, R. Balanced Basis Sets of Split Valence, Triple Zeta Valence and Quadruple Zeta Valence Quality for H to Rn: Design and Assessment of Accuracy. *Phys. Chem. Chem. Phys.* **2005**, *7*, 3297-3305.
- (26) Monkhorst, H. J.; Pack, J. D. Special Points for Brillouin-Zone Integrations. *Phys. Rev. B* **1976**, *13*, 5188-5192.
- (27) Pascale, F.; Zicovich-Wilson, C. M.; López Gejo, F.; Civalleri, B.; Orlando, R.; Dovesi, R. The Calculation of the Vibrational Frequencies of Crystalline Compounds and its Implementation in the CRYSTAL Code. *J. Comput. Chem.* **2004**, *25*, 888-897.
- (28) Zicovich-Wilson, C. M.; Pascale, F.; Roetti, C.; Saunders, V. R.; Orlando, R.; Dovesi, R. Calculation of the Vibration Frequencies of α -Quartz: The Effect of Hamiltonian and Basis Set. *J. Comput. Chem.* **2004**, *25*, 1873-1881.
- (29) Maschio, L.; Kirtman, B.; Orlando, R.; Rérat, M. Ab Initio Analytical Infrared Intensities for Periodic Systems through a Coupled Perturbed Hartree-Fock/Kohn-Sham Method. *J. Chem. Phys.* **2012**, *137*, 204113/1-204113/11.
- (30) Maschio, L.; Kirtman, B.; Rérat, M.; Orlando, R.; Dovesi, R. Ab Initio Analytical Raman Intensities for Periodic Systems through a Coupled Perturbed Hartree-Fock/Kohn-Sham Method in an Atomic Orbital Basis. I. Theory. *J. Chem. Phys.* **2013**, *139*, 164101/1-164101/13.
- (31) Scott, A. P.; Radom, L. Harmonic Vibrational Frequencies: An Evaluation of Hartree-Fock, Møller-Plesset, Quadratic Configuration Interaction, Density Functional Theory, and Semiempirical Scale Factors. *J. Phys. Chem.* **1996**, *100*, 16502-16513.
- (32) Alecu, I. M.; Zheng, J.; Zhao, Y.; Truhlar, D. G. Computational Thermochemistry: Scale Factor Databases and Scale Factors for Vibrational Frequencies obtained from Electronic Model Chemistries. *J. Chem. Theory. Comput.* **2010**, *6*, 2872-2887.
- (33) Setyawan, W.; Curtarolo, S. High-Throughput Electronic Band Structure Calculations: Challenges and Tools. *Comp. Mat. Sci.* **2010**, *49*, 299-312.
- (34) Momma, K.; Izumi, F. VESTA 3 for Three-Dimensional Visualization of Crystal, Volumetric and Morphology Data. *J. Appl. Crystallogr.* **2011**, *44*, 1272-1276.
- (35) Noori, K.; Giustino, F. Ideal Energy-Level Alignment at the ZnO/P3HT Photovoltaic Interface. *Adv. Funct. Mater.* **2012**, *22*, 5089-5095.

- (36) Xu, Y.; Hofmann, O. T.; Schlesinger, R.; Winkler, S.; Frisch, J.; Niederhausen, J.; Vollmer, A.; Blumstengel, S.; Henneberger, F.; Koch, N.; Rinke, P.; Scheffler, M. Space-Charge Transfer in Hybrid Inorganic-Organic Systems. *Phys. Rev. Lett.* **2013**, *111*, 226802/1-226802/5.
- (37) Hofmann, O. T.; Atalla, V.; Moll, N.; Rinke, P.; Scheffler, M. Interface Dipoles of Organic Molecules on Ag(111) in Hybrid Density-Functional Theory. *New. J. Phys.* **2013**, *15*, 123028/1-123028/25.
- (38) Hofmann, O. T.; Deinert, J. -.; Xu, Y.; Rinke, P.; Stähler, J.; Wolf, M.; Scheffler, M. Large Work Function Reduction by Adsorption of a Molecule with a Negative Electron Affinity: Pyridine on ZnO (101⁻0). *J. Chem. Phys.* **2013**, *139*, 174701/1-174701/10.
- (39) Abrahams, S. C.; Bernstein, J. L. Remeasurement of Structure of Hexagonal ZnO. *Acta Cryst.* **1969**, *B 25*, 1233-1236.
- (40) Wöll, C. The Chemistry and Physics of Zinc Oxide Surfaces. *Prog Surf Sci* **2007**, *82*, 55-120.
- (41) Tanskanen, J. T.; Häggglund, C.; Bent, S. F. Correlating Growth Characteristics in Atomic Layer Deposition with Precursor Molecular Structure: The Case of Zinc Tin Oxide. *Chem. Mater.* **2014**, *26*, 2795-2802.
- (42) Hill, J. G.; Platts, J. A.; Werner, H. J. Calculation of Intermolecular Interactions in the Benzene Dimer using Coupled-Cluster and Local Electron Correlation Methods. *Phys. Chem. Chem. Phys.* **2006**, *8*, 4072-4078.
- (43) Meyer, B.; Marx, D.; Dulub, O.; Diebold, U.; Kunat, M.; Langenberg, D.; Wöll, C. Partial Dissociation of Water Leads to Stable Superstructures on the Surface of Zinc Oxide. *Angew. Chem. Int. Ed.* **2004**, *43*, 6642-6645.
- (44) Wang, Y.; Muhler, M.; Wöll, C. Spectroscopic Evidence for the Partial Dissociation of H₂O on ZnO(101⁻0). *Phys. Chem. Chem. Phys.* **2006**, *8*, 1521-1524.
- (45) Calzolari, A.; Nardelli, M. B. Dielectric Properties and Raman Spectra of ZnO from a First Principles Finite-differences/finite-Fields Approach. *Sci. Rep.* **2013**, *3*, 2999/1-2999/6.
- (46) Klingshirn, C. ZnO: Material, Physics and Applications. *ChemPhysChem* **2007**, *8*, 782-803.
- (47) Betzinger, M.; Friedrich, C.; Blügel, S. Hybrid Functionals within the all-Electron FLAPW Method: Implementation and Applications of PBE0. *Phys. Rev. B* **2010**, *81*, 195117/1-195117/13.
- (48) Marsman, M.; Paier, J.; Stroppa, A.; Kresse, G. Hybrid Functionals Applied to Extended Systems. *J. Phys. : Condens. Matter* **2008**, *20*, 064201/1-064201/9.
- (49) Oba, F.; Togo, A.; Tanaka, I.; Paier, J.; Kresse, G. Defect Energetics in ZnO: A Hybrid Hartree-Fock Density Functional Study. *Phys. Rev. B* **2008**, *77*, 245202/1-245202/6.
- (50) Dominguez, A.; Lorke, M.; Schoenhalz, A. L.; Rosa, A. L.; Frauenheim, T.; Rocha, A. R.; Dalpian, G. M. First Principles Investigations on the Electronic Structure of Anchor Groups on ZnO Nanowires and Surfaces. *J. Appl. Phys.* **2014**, *115*, 203720/1-203720/9.
- (51) Malm, J.; Sahramo, E.; Perälä, J.; Sajavaara, T.; Karppinen, M. Low-Temperature Atomic Layer Deposition of ZnO Thin Films: Control of Crystallinity and Orientation. *Thin Solid Films* **2011**, *519*, 5319-5322.

For Table of Contents Only

